Magneto-optical spectra of Fe/Au artifical superlattices modulated by integer and noninteger atomic layers

Katsuaki Sato,[a] Eishi Takeda, and Masanori Akita
Faculty of Technology, Tokyo University of Agriculture and Technology, Koganei, Tokyo 184-8588, Japan

Masatake Yamaguchi
Center for Promotion of Computational Science and Engineering, Japan Atomic Energy Research Institute, Tokai-mura, Ibaraki 319-1195, Japan

Koki Takanashi, Seiji Mitani, and Hiroyasu Fujimori
Institute for Materials Research, Tohoku University, Katahira, Aoba-ku, Sendai, Miyagi 980-8577, Japan

Yoshishige Suzuki
Joint Research Center for Atom Technology, Tsukuba, Ibaraki 305-8562, Japan

(Received 27 March 1998; accepted for publication 24 July 1999)

Spectra of the magneto-optical Kerr effect, in a series of $[\mathrm{Fe}\,(x\mathrm{ML})/\mathrm{Au}\,(x\mathrm{ML})]_N$ superlattices with integer and noninteger values of x ($1 \leqslant x \leqslant 15$), were measured. For $x=1$ the superlattic forms an $L1_0$-type ordered alloy structure. The magneto-optical spectrum of the superlattice exhibits a prominent structure around 4 eV, which shows a systematic shift toward higher energies as x increases ($1 \leqslant x \leqslant 5$). No such structure can be reproduced by an optical calculation assuming a simple stack of thin Fe and Au layers. *Ab initio* band calculations have shown similar magneto-optical spectra and a similar peak shift with an increase in x ($1 \leqslant x \leqslant 6$). This suggests that electronic structures which differ from that of a simple stack of thin Fe and Au are realized in the superlattices. For noninteger values of x, oscillatory behavior with a period of one monolayer was observed in the low energy region of the magneto-optical spectra. © *1999 American Institute of Physics.* [S0021-8979(99)03121-7]

INTRODUCTION

Recent developments in epitaxial growth technology have made it possible to fabricate artificial structures on an atomic scale.[1] Artificial structures (superlattices or sandwiches) consisting of magnetic and nonmagnetic thin layers have been attracting interest as new functional materials with novel physical properties such as giant magneto-resistance (GMR), large surface magnetic anisotropy and unusual magneto-optical (MO) responses. In particular, one of the authors has observed characteristic structures in the MO spectra of ultrathin Fe layers sandwiched by Au layers, and has attributed the spectral structure to the quantum confinement effect of electrons with a certain spin direction.[2] A similar quantum confinement effect is also expected to occur in multilayers consisting of Fe and Au. One question that these experiments can also address is the effect on the electronic structure when the thickness of the constituent layer becomes mono atomic in size. Hybridization of electron orbitals with those of adjacent layers should result in an electronic structure different from that of the bulk.

Motivated by this one of the authors and his collaborators fabricated $[\mathrm{Fe}\,(1\,\mathrm{ML})/\mathrm{Au}\,(1\,\mathrm{ML})]_N$ superlattices by alternately depositing monolayers of Fe (001) and Au (001). This superlattice forms an $L1_0$-type ordered structure, and the long-range order parameter is estimated to be 0.5 from the intensity ratio of the superlattice (001) peak to the fundamental (002) peak in the x-ray diffraction.[3,4] Figure 1 shows the atomic arrangement in a unit cell of the $L1_0$ structure. Fabrication of such an "ordered alloy" structure is quite remarkable, since the Fe–Au system belongs to a peritectic-type phase diagram, which rules out the existence of either intermetallic compounds or intermediate alloys. Magnetic measurements revealed that the magnetic moment per one Fe atom is approximately equal to 2.8 μ_B, which is much larger than the value of 2.2 μ_B for pure body-centered-cubic (bcc) Fe. The magneto-optical Kerr effect (MOKE) was measured for this $L1_0$-type alloy to provide insight into the electronic structure of this material.[5] The resulting MOKE spectrum showed a characteristic structure around 4 eV that had not been observed either in a single Fe film or in a Fe/Au multilayer with a long modulation period.

When the modulation period x is increased,[4,6] the Fe moment still remains at an enhanced value of nearly 2.7 μ_B for $x \leqslant 3$. In addition, $t_{\mathrm{Fe}}K_u$, in which K_u is the magnetic anisotropy constant and t_{Fe} is the thickness of a Fe layer, is found to obey a linear relationship with x,[7] as has been reported in many multilayer systems.[8] MOKE spectra in the series of $[\mathrm{Fe}\,(x\mathrm{ML})/\mathrm{Au}\,(x\mathrm{ML})]_N$ superlattices for $1 < x \leqslant 15$ show a systematic variation of spectral features. For small periods ($x \leqslant 5$) the spectral shape is quite similar to that of the $L1_0$ alloy with the main peak shifting toward higher energies, while for large periods ($x \geqslant 10$) it was quite similar to that expected from a simulation assuming a simple stack of Fe and Au layers.[9] The characteristic 4 eV structure in the MOKE spectra showed a very similar peak shift with

[a]Electronic mail: satokats@cc.tuat.ac.jp

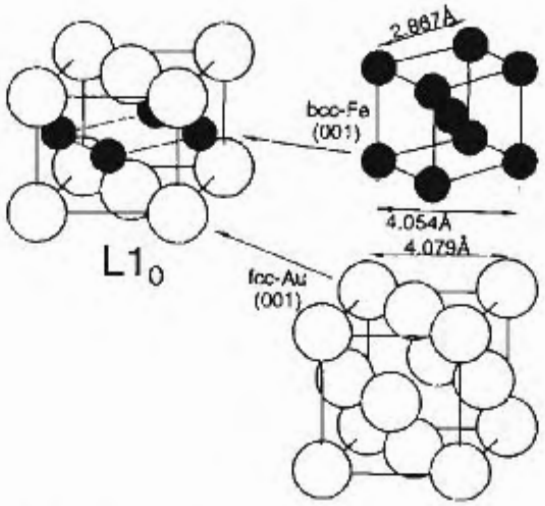

FIG. 1. Atomic arrangement in a unit cell of Fe–Au with a $L1_0$ structure

increasing modulation period x, as observed in the MOKE spectra of ultrathin Fe layers sandwiched by Au.[10]

Electronic energy band structures of $[Fe(x\text{ML})/Au(x\text{ML})]_N$ superlattices for integer x ($1 \leqslant x \leqslant 6$) were calculated by one of the authors by means of the linearized muffin-tin orbital method with atomic sphere approximation (LMTO-ASA) method. MOKE spectra were estimated using wave functions obtained by the calculation. The resultant spectra exhibit prominent MO structures around 4 eV, which is ascribed to an optical transition from the Au $5d$ states to the Au $5f$ states hybridized with the Fe $3d$ states in the minority spin band.[11]

Recently, $[Fe(x\text{ML})/Au(x\text{ML})]_N$ superlattices modulated by noninteger number ($x = 1.25, 1.5, 1.75, \ldots$) of atomic layers were also prepared. XRD measurements indicate that coherent layered structures are formed even in the noninteger case.[12] It was also found that the lattice constants and the perpendicular magnetic anisotropy show oscillatory behavior for noninteger values of x between 1 and 4.[13,14] Oscillatory behavior of a MOKE structure with the modulation period x in the low photon energy region was also observed.[15]

In this article, we present an overview of our MO studies in $[Fe(x\text{ML})/Au(x\text{ML})]_N$ superlattices with integer and noninteger values of x and discuss a general trend in the variation of the electronic structure of the superlattice series. A part of this study has been published elsewhere.

II. EXPERIMENT

The specimens used in the present study were prepared on MgO (100) substrates by an ultrahigh vacuum (UHV) deposition technique. The base pressure of the deposition system was 3×10^{-10} Torr. A Fe seed layer of 1 nm followed by a Au buffer layer of 50 nm was deposited at 200 °C and subsequently annealed for 30 min to 1 h at 500 °C. The orientation of the Au buffer layer was (001). The Fe seed was necessary to control the orientation of the Au layer. Multilayers with N periods, with each period consisting of x ML Fe and x ML Au, were deposited in the UHV system at 70 °C on the Au buffer. The parameter x took either integer ($x = 1, 2, 3, 4, 5, 6, 8, 10$ and 15) or noninteger numbers ($x = 1.25, 1.5, 1.75, 2.25, 2.5, 2.75, 3.25, 3.5$ and 3.75). The crystallographic plane of the Fe film on Au (100) was determined as (001). The deposition rates were approximately 0.01 nm/s. Superlattices with noninteger modulation were also fabricated on the Au (100) surface. The layer thickness was controlled using a quartz thickness monitor. Details of these preparation techniques are given elsewhere.[3,4,6]

TABLE I. Structure parameters of $[Fe(x\text{ML})/Au(x\text{ML})]_N$ multilayers with integer and noninteger x

x (ML)	N (periods)	Thickness for one period (nm)	Observed d_{002} value (nm)
1	100	0.3840	0.1915
2	50	0.7272	0.1812
3	33	1.0744	0.1785
4	25	1.4216	0.1770
5	20	1.7688	0.1795
6	17	2.116	0.1760
8	13	2.8104	0.1755
10	10	3.5048	0.1728
15	7	5.2408	0.1698
1.25	30	0.4324	0.1775
1.50	30	0.4845	0.1745
1.75	57	0.5865	0.1795
2.25	30	0.8544	0.179
2.50	30	0.8963	0.176
2.75	36	0.9605	0.178
3.25	30	1.1428	0.1771
3.50	30	1.2726	0.1761
3.75	30	1.3007	0.1772

Epitaxial growth of the Fe/Au multilayers was confirmed by (RHEED) patterns for both series of samples. The repetition number N, the average lattice-plane spacing normal to the film plane obtained by XRD, as well as the observed $d_{(002)}$ spacing for each superlattice are listed in Table I.

Spectra of the MOKE were measured at room temperature between 1.2 and 6 eV employing a Kerr spectrometer with a polarization modulation technique using a photoelastic modulator (PEM).[16] The measurements provided both Kerr rotation and ellipticity spectra. The samples were saturated with a perpendicular magnetic field with a flux density of 1.7 T. The optical reflectivity was measured using a Hitachi U-3410 spectrophotometer from which optical constants were calculated by Kramers-Kronig analysis and helped in the optical constants measurements by a Woollam type WVASE spectroscopic ellipsometer between 2 and 5 eV.

III. STRUCTURE CHARACTERIZATION

The $[Fe(x\text{ML})/Au(x\text{ML})]_N$ films obtained were characterized by XRD. The $x = 1$ superlattice, i.e., the $[Fe(1\text{ML})/Au(1\text{ML})]_{100}$ clearly showed a diffraction line ($2\theta = 22.9°$) characteristic of the tetrahedral $L1_0$ ordered structure. For Fe/Au multilayers with thicker layers, i.e. $[Fe(x\text{ML})/Au(x\text{ML})]_N$ ($x = 2-15$), satellite lines due to the multilayer structure were also observed. Figure 2 shows XRD profiles measured using Cu $K\alpha$ radiation for $x = 1, 2, 3$ and 4. In addition to the (002) diffraction peaks ascribed to MgO substrates and Au buffers, a single peak was observed

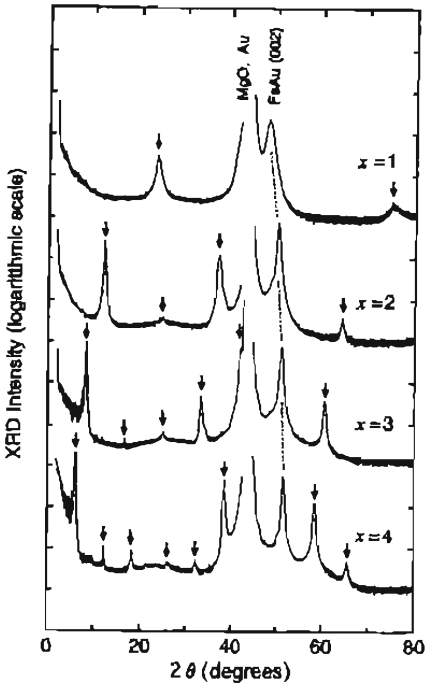

FIG. 2. θ-2θ XRD profiles taken with Cu $K\alpha$ radiation for $[\mathrm{Fe}\,(x\mathrm{ML})/\mathrm{Au}\,(x\mathrm{ML})]_N$ superlattices with $x=1$, 2, 3 and 4. The arrows indicate satellites due to superlattice structures. The intensity is expressed on the logarithmic scale.

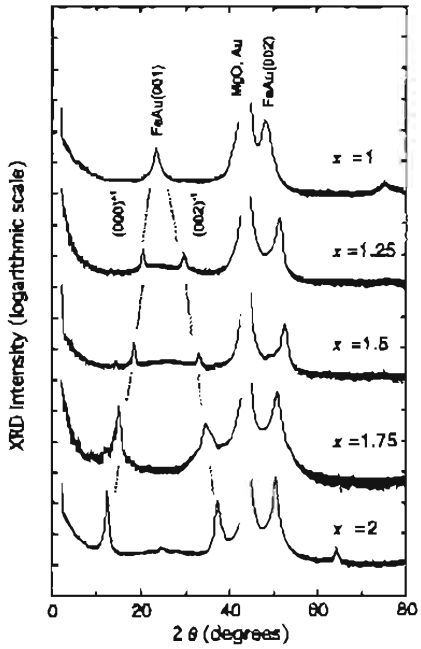

FIG. 3. θ-2θ XRD profiles taken with Cu $K\alpha$ radiation for $[\mathrm{Fe}\,(x\mathrm{ML})/\mathrm{Au}\,(x\mathrm{ML})]_N$ superlattices with $x=1$, 1.25, 1.5, 1.75 and 2. The labels (000)+1 and (002)−1 represent the first-order satellite peak of the fundamental (000) peak and the minus first-order satellite peak of the fundamental (002) peak, respectively. The intensity is expressed on a logarithmic scale.

at a diffraction angle between bcc Fe (002) and face-centered-cubic (fcc) Au (002), while no peaks corresponding to other crystal orientations were detected. The fundamental (002) peaks were accompanied by various satellite peaks characteristic of superlattice structures. This indicates that a coherent stacking of Fe [001] and Au [001] layers is formed. In particular, for $x=1$ the satellite peaks at $2\theta=22.9°$ and 73.7° are very pronounced, and can be assigned to (001) and (003) superlattice peaks, respectively, in the $L1_0$ ordered structure.

Figure 3 shows XRD profiles for $x=1$, 1.25, 1.5, 1.75 and 2. As x increases from 1, the (001) peak appears to split into two separate peaks, and the positions of the peaks vary systematically with x, smoothly approaching the superlattice peaks for $x=2$. We consider that these two peaks correspond to the first-order satellites of the fundamental (000) and (002) peaks. The important point is that these peaks have a narrow linewidth, from which the coherence length is estimated to be comparable with the total thickness of the film.

To simulate the x-ray diffraction profiles, we propose a model for the fractional superlattice assuming complete layer-by-layer growth. Here we also assume that structural coherence is maintained throughout the sample. The fraction of the sites occupied by Fe atoms, r_{Fe}, is illustrated in Fig. 4 as a function of the atomic layer number for $x=1.0$, 1.25, 1.5 and 1.75. As an example, consider the case of $x=1.25$. The deposition of Fe 1.25 ML results in a full occupancy of Fe atoms in the first atomic layer, and a one quarter occupancy in the second atomic layer with the excess Fe atoms. The subsequent deposition of Au 1.25 ML leads to occupation of the remaining free site equivalent to 0.75 ML in the second atomic layer, with one half occupancy in the third atomic layer by the remainder of the Au atoms. In this way, the composition changes systematically with the atomic layer number due to the existence of the fractional atomic layer, i.e., 0.25 ML for $x=1.25$, 0.5 ML for $x=1.5$, and 0.75 ML for $x=1.75$.

The x-ray structure factor is expressed by

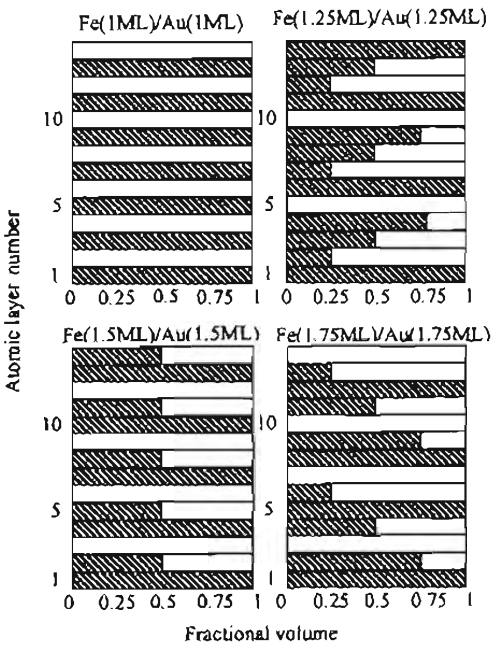

FIG. 4. Schematic diagram showing the fractional occupation of Fe atoms in the layers of superlattices with $x=1.25$, 1.5 and 1.75, assuming coherent layer-by-layer growth for the $\mathrm{Fe}\,(x\mathrm{ML})/\mathrm{Au}\,(x\mathrm{ML})$ superlattice.

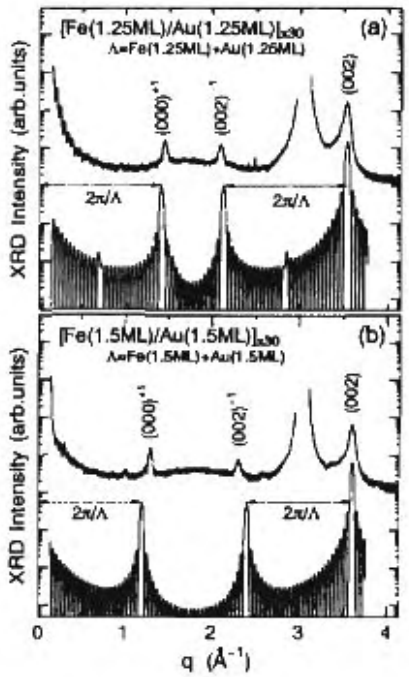

FIG. 5. Experimental XRD profiles and the square of the x-ray scattering factor calculated from the coherent layer-by-layer growth model for (a) [Fe (1.25 ML)/Au (1.25 ML)]$_{30}$ and (b) [Fe (1.5 ML)/Au (1.5 ML)]$_{30}$.

$$F(q)=S_n f_n \exp(iqz_n), \tag{1}$$

where q and z_n are the absolute values of the scattering vector $\mathbf{q}$ and the position of the nth atomic layer, respectively, and f_n the scattering factor of the nth atomic layer, given by

$$f_n=r_{Fe}f_{Fe}+(1-r_{Fe})f_{Au}. \tag{2}$$

Here f_{Fe} and f_{Au} are the atomic scattering factors of Fe and Au, respectively.

Results of experiments and calculations are compared in Figs. 5(a) and 5(b) for $x=1.25$ and 1.5, respectively. The results of the calculations are in an excellent agreement with those of the experiments, suggesting formation of a coherent layered structure even for noninteger values of x.

IV. OPTICAL INVESTIGATIONS IN Fe/Au SUPERLATTICES MODULATED BY INTEGER ATOMIC LAYERS

A. MOKE spectra

MOKE spectra of [Fe (xML)/Au (xML)]$_N$ films with an integer number of x ($1\leqslant x\leqslant 15$) are shown separately in Figs. 6 and 7 for $x=1$, 2, 3, 4, 5 and $x=6$, 8, 10 15, respectively. In Figs. 6 and 7 both Kerr rotation θ_K and Kerr ellipticity η_K are plotted.

As shown in Fig. 6(a) the spectrum of Kerr rotation θ_K for $x=1$ shows two humps located around 1.5 and 3 eV followed by a negative slope, a change in sign at 3.7 eV and a negative peak at 4.3 eV. The curve crosses zero again at 4.8 eV and increases with photon energy up to the highest energy of the measurement, 6 eV. The negative peak of θ_K or the position of the negative slope of η_K shifts towards higher energies with an increase in x, i.e., the peak position moves as 4.6→4.9→5.1→5.5 eV for the change of the

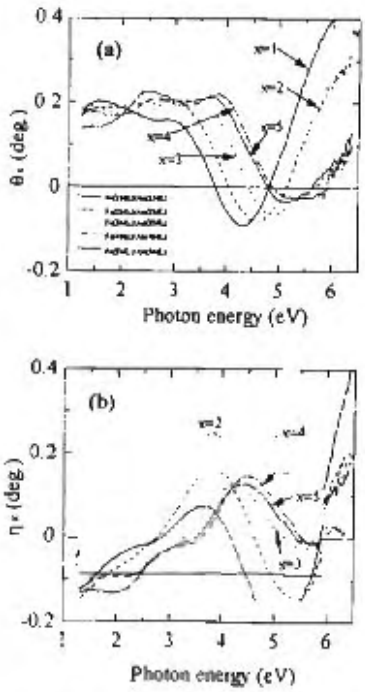

FIG. 6. Magneto-optical spectra in [Fe (xML)/Au (xML)]$_N$ superlattices for $x=1-5$. (a) Kerr rotation and (b) Kerr ellipticity

modulation period $x=2\rightarrow3\rightarrow4\rightarrow5$ (Fig. 6). A slight hump is found around 5 eV for $x\geqslant6$ as shown in Fig. 7(a), and a positive peak around 4 eV becomes quite prominent for $x=6$ and 8, and then disappears for larger values of x.

Another structure is observed at around 2.2–2.4 eV in Fig. 7 for $x\geqslant6$, i.e., a distinct peak in the Kerr rotation, or a corresponding dispersion-type line shape. This peak has been attributed to an *enhancement effect due to plasma resonance* by Au layers. It is well known that the complex Kerr rotation

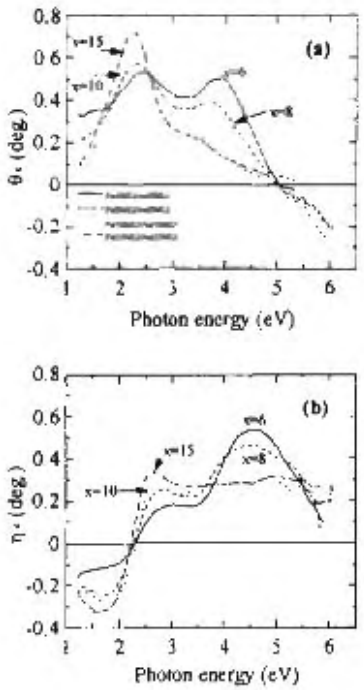

FIG. 7. Magneto-optical spectra in [Fe (xML)/Au (xML)]$_N$ superlattices for $x=6-15$. (a) Kerr rotation and (b) Kerr ellipticity

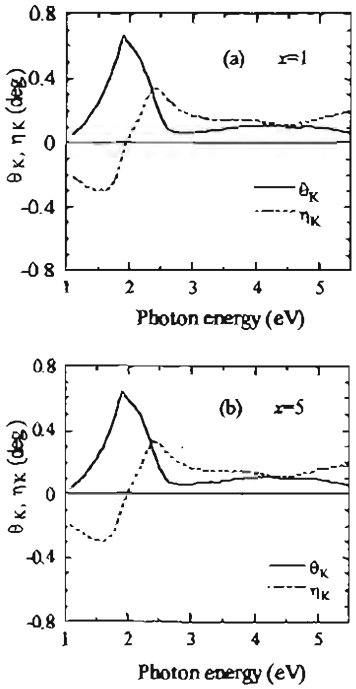

FIG. 8. Simulated magneto-optical spectra of $[\mathrm{Fe}\,(x\mathrm{ML})/\mathrm{Au}\,(x\mathrm{ML})]_N$ for x (a) 1 and (b) 5

$\Phi_K = \theta_K + i\,\eta_K$ is associated with the off-diagonal as well as the diagonal element of the dielectric tensor (or the conductivity tensor) as follows.[17]

$$\Phi_K = \frac{\epsilon_{xy}}{\sqrt{\epsilon_{xx}}(1-\epsilon_{xx})} = \frac{-\sigma_{xy}}{\sigma_{xx}\sqrt{1+i4\pi\sigma_{xx}/\omega}}. \tag{3}$$

This expression suggests that complex Kerr rotation can be strongly influenced by the denominator, especially when the expression $|\epsilon_{xx}| \approx 0$ holds or any rapid change occurs in $|\epsilon_{xx}|$. The former case has been referred to as plasma enhancement.[18] Since ϵ'_{xx} does not cross zero around 2.4 eV (as will be shown later in Fig. 10), the MOKE structure around this photon energy 2.4 eV may be due to enhancement by a rapid change of the optical constant in the Au layers, caused by an onset of interband transitions.

Magneto-optical spectra were simulated using the virtual optical constant method[19] assuming a simple stack of Fe and Au layers with the bulk values of diagonal and off-diagonal elements.[20] Typical results of calculation for $x=1$ and 5 are shown in Figs. 8(a) and 8(b), respectively.[5] A Kerr rotation peak can be seen at around 1.9 eV due to the above-mentioned enhancement effect, regardless of the layer thickness. The simulated spectra were completely different from the experimental Kerr spectra for $x \leqslant 5$, shown in Fig. 6(a). This clearly suggests that the electronic structure of Fe/Au superlattices with an ultra thin modulation period is substantially different from that of a simple stack of Fe and Au layers. However, the MOKE spectra for $x \geqslant 10$, shown in Fig. 7(a), are quite similar to the simulated spectra shown in Fig. 8, although the peak position (1.9 eV) of the simulated spectrum is slightly lower than that (2.4 eV) of the observed spectra for $x=15$. Therefore, the superlattice with $x \geqslant 10$ can be approximated by a simple stack of Fe and Au layers. The discrepancy in the peak position may be due to the difference in the value of ϵ_{xy} of Fe in ultrathin layers as compared with the bulk value, which was used in the optical simulations.

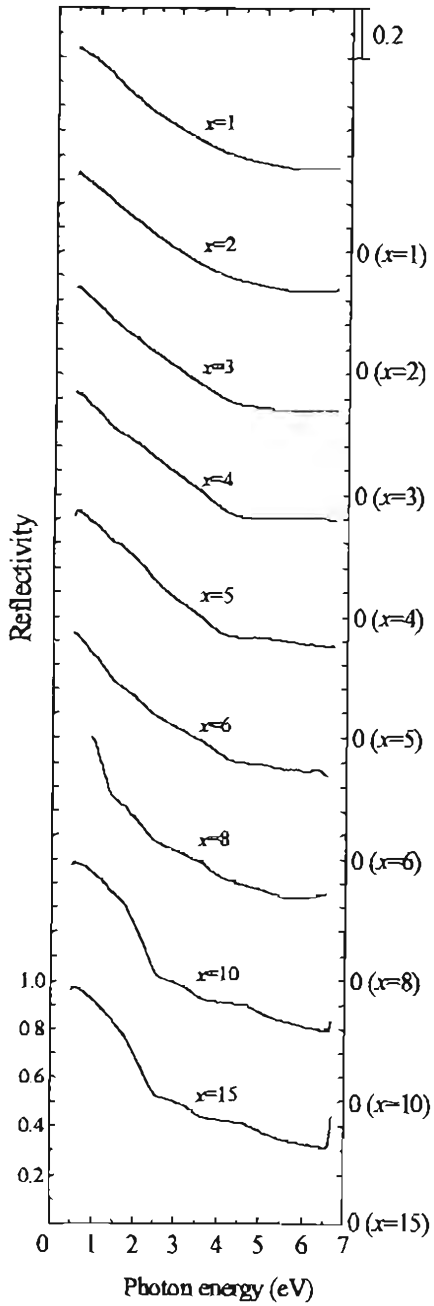

FIG. 9. Reflectivity spectra of $[\mathrm{Fe}\,(x\mathrm{ML})/\mathrm{Au}\,(x\mathrm{ML})]_N$ superlattices for $x = 1-15$ (integer).

B. Reflectivity spectra and dielectric functions

Reflectivity spectra of these superlattices are shown in Fig. 9. The real and imaginary parts of the dielectric function were calculated by Kramers-Kronig analysis of the reflectivity. We used optical constants measured by spectroscopic ellipsometry for photon energies between 2 and 5 eV to determine the extrapolation parameters in the Kramers-Kronig analysis. Real and imaginary parts of the diagonal compo-

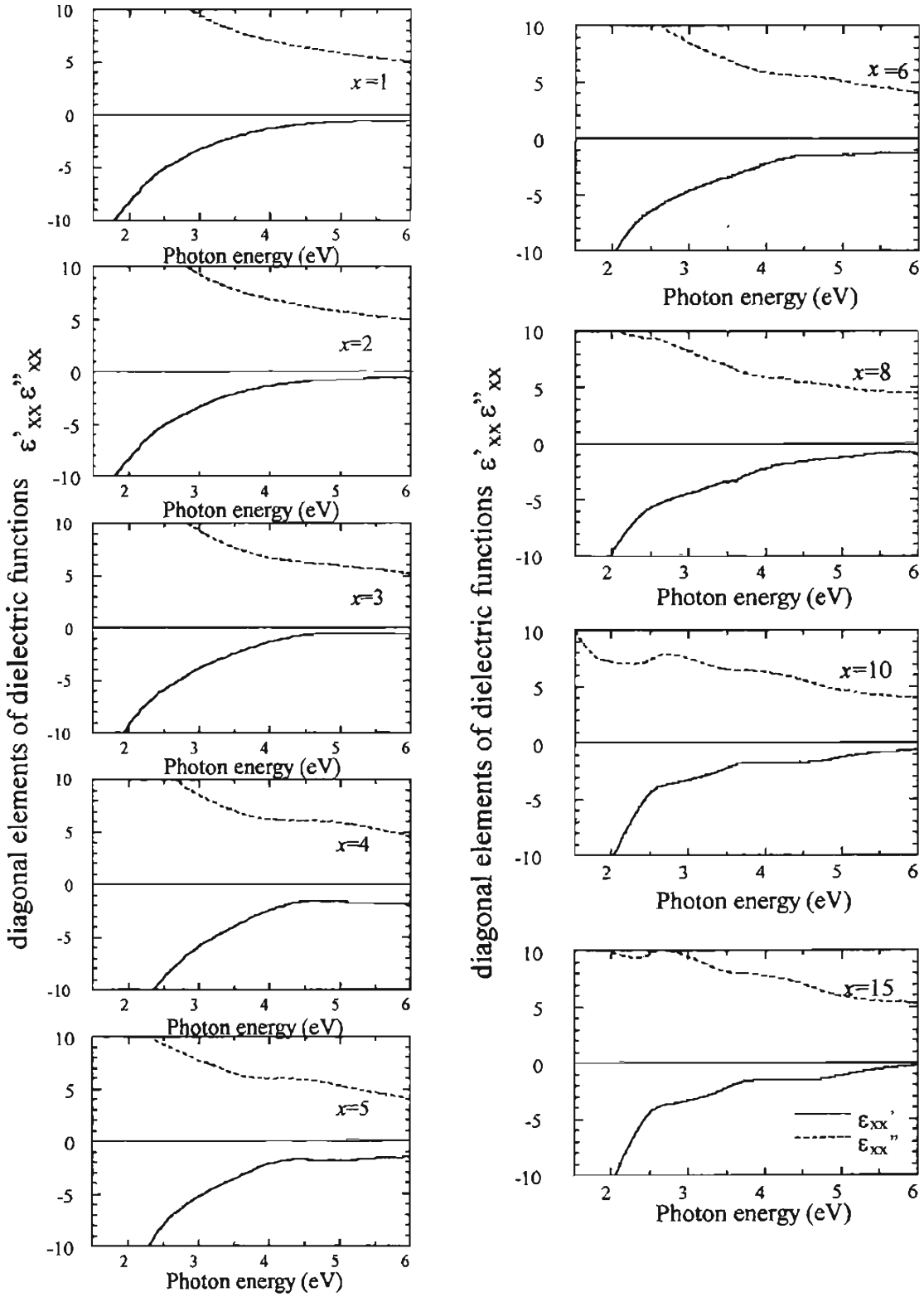

FIG. 10. Spectra of diagonal elements of dielectric functions for $x = 1-15$. The solid curve denotes the real part and the dotted one the imaginary.

nent of the dielectric function in $[\mathrm{Fe}\,(x\mathrm{ML})/\mathrm{Au}\,(x\mathrm{ML})]_N$ are plotted in Fig. 10 for $x = 1-15$, respectively. Only a gradual change in the spectral features is observed throughout the series. For $x = 1$, 2, 3, 4, 5 and 6, a break in the curve of ϵ'_{xx} spectra is observed at 4.7, 4.6, 4.5, 4.2 and 4.3 eV, respectively. On the other hand, for $x = 8$, 10 and 15 the break is also seen at 2.5, 2.5 and 2.6 eV, respectively. The break may be attributed to an onset of interband transitions.

The imaginary part of the off-diagonal element of conductivity tensor multiplied by the angular frequency, i.e., $\omega\sigma''_{xy}$, was determined using experimentally obtained data of θ_K, η_K and ϵ_{xx}. The $\omega\sigma''_{xy}$ parameter is useful for discuss-

ing the origin of the MOKE from the electronic structures, since this quantity can be directly connected with the joint density of states, which will be described later. The spectra thus determined are given in Figs. 11(a) and 11(b) for $1 \leqslant n \leqslant 5$ and $6 \leqslant n \leqslant 15$, respectively.

The spectra of $\omega\sigma''_{xy}$ for $x=1$ to 5 [Fig. 11(a)] all show a peak which undergoes a dramatic shift of the energy position from 4.5 to 5.5 eV. These curves are completely different from the $\omega\sigma''_{xy}$ spectra of Fe reported in the literature.[20] Figure 11(a) also shows a constant offset value of $\omega\sigma''_{xy} = -2\times10^{29}\,s^{-2}$ in the low energy region. Such a constant value in the spectrum of $\omega\sigma''_{xy}$ was attributed to the spin polarization of conduction electrons, according to Erskine and Stern.[21]

On the other hand, the spectra for $x=6-15$ [Fig. 11(b)] are comprised of two peaks, one located around 2–2.5 eV and the other around 4 eV. The spectral feature is quite similar to that of Fe, except for the peak position (2.5 eV) of the lower energy peak, which is located at a slightly higher energy than that of Fe. A distinct peak at around 4 eV appears for $x=6$ and 8. The intensity of the peak is twice as large as the corresponding peak for $x=1$.

It is obvious from Fig. 11(a) that the electronic structure of the $L1_0$-type Fe/Au superlattices involves significant hybridization between Fe and Au orbitals. The electronic structure of a Fe layer in $[\mathrm{Fe}(1\,\mathrm{ML})/\mathrm{Au}(1\,\mathrm{ML})]_N$ is modified from that of bulk Fe since the d orbitals in the Fe layer overlap those of neighboring Au orbitals. The electronic structure of Au in the superlattice will also be different from bulk Au.

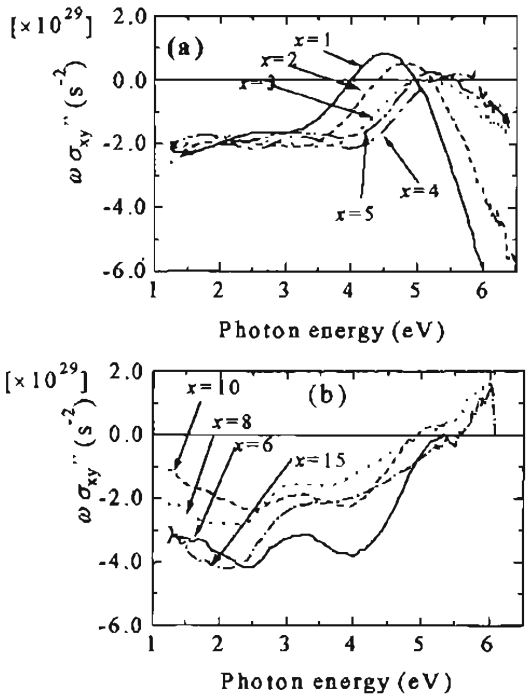

FIG. 11. Spectra of the imaginary part of the off-diagonal conductivity tensor element multiplied by the angular frequency in Fe/Au superlattices for x=(a) 1–5 and (b) 6–15.

V. CALCULATION OF MOKE SPECTRA FROM BAND THEORY

Calculations of the electronic structure of the Fe/Au superlattices were performed within the framework of the local spin density approximations to the density functional theory[22] using the LMTO-ASA method including the relativistic effects in a perturbative way. First, the scalar-relativistic electronic structure ignoring spin-orbit interaction was calculated. Second, the spin-orbit Hamiltonian was included self-consistently by assuming the magnetization direction along ⟨001⟩ axis. The cut off of angular momentum (l_{max}) was chosen to be 3.

The real part of the diagonal optical conductivity tensor $[\mathrm{Re}(\sigma_{xx})]$ and the imaginary part of the off-diagonal one $[\mathrm{Im}(\sigma_{xy})]$ were calculated from the following formula derived by Wang and Callaway,[23]

$$\mathrm{Re}[\sigma_{xx}(\omega)] = \frac{\pi e^2}{m^2\hbar\omega}\sum_{lk}^{\mathrm{occ}}\sum_{nk}^{\mathrm{unocc}}\left|\prod_{\ln k}^{x}\right|^2\delta(\omega-\omega_{\ln k}), \tag{4}$$

$$\mathrm{Im}[\sigma_{xy}(\omega)] = \frac{\pi e^2}{m^2\hbar\omega}\sum_{lk}^{\mathrm{occ}}\sum_{nk}^{\mathrm{unocc}}\mathrm{Im}\left(\prod_{\ln k}^{y}\prod_{nlk}^{x}\right) \times\delta(\omega-\omega_{\ln k}). \tag{5}$$

Here, $\hbar\omega_{\ln k}=E_n(k)-E_l(k)$ is the energy difference between the occupied (l) and unoccupied band (n) at a sampling $\mathbf{k}$ point in the first Brillouin zone and $\Pi^{\alpha}_{\ln k}$ ($\alpha=x,y$) is the transition matrix element given by

$$\prod_{\ln k}^{\alpha} = \langle nk|p_\alpha|lk\rangle, \tag{6}$$

with $|lk\rangle$ the Bloch state, $\mathbf{k}$ the wave vector, and P_α the α^{th} component of the momentum operator.

$\mathrm{Im}[\sigma_{xx}(\omega)]$ and $\mathrm{Re}[\sigma_{xy}(\omega)]$ were calculated using a Kramers-Kronig transformation from $\mathrm{Im}[\sigma_{xx}(\omega)]$ and $\mathrm{Re}[\sigma_{xy}(\omega)]$, respectively. For the interband relaxation parameter, $\gamma=0.5$ eV was used.

The calculated results of the Kerr spectra and $\mathrm{Im}(\omega\sigma_{xy})$ spectra for $\mathrm{Fe}(x\mathrm{ML})/\mathrm{Au}(x\mathrm{ML})$ ($x=1-6$) are shown in Figs. 12 and 13, respectively. The sign of Kerr rotation is reversed from that of the other experimental figures due to the different sign convention adopted in the theoretical calculations. In the case of $x=1$, the crystal structure is an ordered $L1_0$-type structure. In our calculated results, the peak structure at about 4 eV shifts towards higher energies and the large Kerr angle around 6 eV decreases with an increase of x. These trends are in good agreement as a whole with the experimental data.

From the detailed analysis of the band structure and transition matrix elements, it was found that the peak structure around 4 eV in the case of $x=1$ originates mainly from the $d_\downarrow \rightarrow f_\downarrow$ transition at the atomic site of Au, in which the final state $f_\downarrow$ is the one hybridized with the $\mathrm{Fe}(3d_\downarrow)$ state. In other words, this transition can be regarded as the $\mathrm{Au}(5d_\downarrow) \rightarrow \mathrm{Fe}(3d_\downarrow)$ transition. One of the authors proposed the assignment from a simple analysis using density of states function.[9]

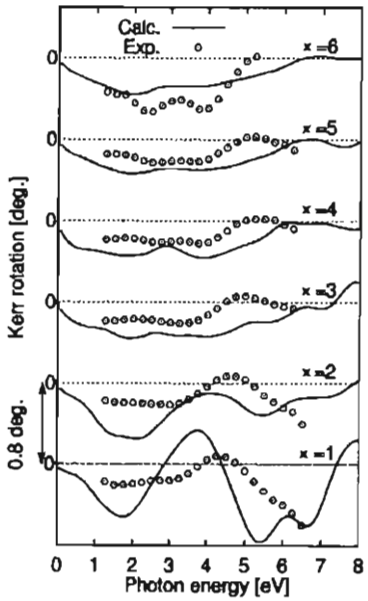

FIG. 12. Calculated and experimental MOKE spectra of $[\mathrm{Fe}(x\mathrm{ML})/\mathrm{Au}(x\mathrm{ML})]_N$ ($x=1-6$) superlattices. (The sign of the vertical axis is reversed from that shown in Fig. 6. This is due to a different sign convention adopted in the theoretical calculation.)

The peak structure around 4 eV shifts towards higher energies with an increase of x as stated above. From the analysis of the band structure, this is considered to be due to the shift of the final state towards higher energies. However, the calculated peak structure becomes very small in the case of $x=2$, and almost disappears in the case of $x=3$ and more. This drastic change between $x=1$ and 2 is not seen in the experimental results. A similar situation is also found in the calculated and experimental magnetic moments. The calculated magnetic moments per Fe atom are 3.07, 2.59, 2.59, 2.56, 2.49, 2.44 μ_B for $x=1$, 2, 3, 4, 5, 6, respectively,

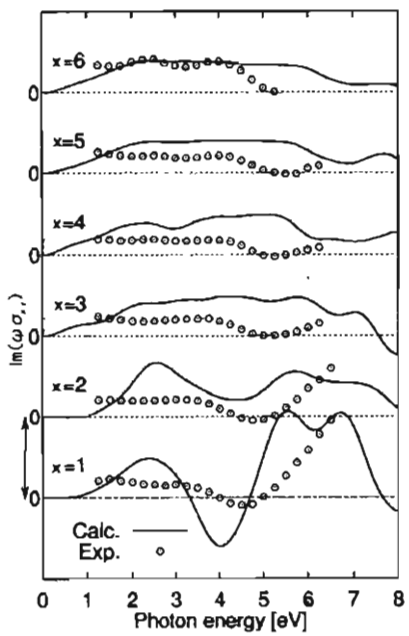

FIG. 13. Calculated and experimental spectra of $\omega\sigma''_{xy}$ of $[\mathrm{Fe}(x\mathrm{ML})/\mathrm{Au}(x\mathrm{ML})]_N$ ($x=1-6$) superlattices.

whereas the experimental ones are 2.75, 2.64, 2.68, 2.72 μ_B for $x=1$, 2, 3, and 4, respectively, with error bars $\pm 0.25\,\mu_B$. Although the calculated magnetic moments show a drastic decrease between $x=1$ and 2, such a trend is not seen in the experiments. The above-mentioned disagreement in Kerr spectra seems to be related to the discrepancy in the magnetic moment. This can be quite reasonably understood since the Au($5d\downarrow$)→Fe($3d\downarrow$) transition may be strongly influenced by the unoccupied Fe($3d\downarrow$) band, which is the final state of the transition and simultaneously determines the size of magnetic moments.

VI. SHIFT OF THE MOKE STRUCTURE WITH THE MODULATION PERIOD

When the modulation period becomes larger ($x \geqslant 6$), the d states of the Fe atoms no longer experience the periodic potential, since the spatial extent of these states is only a few atomic radii. In such a case the quantum confinement of electrons in an individual layer takes place instead of forming the energy band. Present experiments suggest that the critical value of x which discriminates the quantum confinement scheme from the band scheme is around 4.

In ultrathin Fe layers sandwiched by Au, the MOKE spectrum shows a characteristic peak around 3–5 eV, which shifts towards lower energies with a decrease in the layer thickness.[24] This phenomenon was interpreted in terms of the quantum confinement effect of $3d$ electrons in the ultrathin Fe layer.[2,25]

In order to compare the MOKE spectra of the $[\mathrm{Fe}(x\mathrm{ML})/\mathrm{Au}(x\mathrm{ML})]_N$ superlattices obtained in this study with the spectra of Au/Fe/Au sandwiches reported in Ref. 25, we calculated $|\omega\sigma_{xy}| = \sqrt{(\omega\sigma'_{xy})^2 + (\omega\sigma''_{xy})^2}$ of the Fe/Au superlattices. As shown in Fig. 14 two peaks marked by arrows are clearly observed over all the series of spectra, one in the *high-energy* (≈3–5 eV) region and the other in the *low-energy* (≈2 eV) region. The high-energy peak undergoes a substantial shift with x, while the low-energy peak shows only a slight downward shift. In Fig. 15 energy positions of the high-energy and low-energy peaks are plotted as a function of the modulation period by open circles and open triangles, respectively. Also, in Fig. 15, the magneto-optical transition energies associated with quantum well states in ultrathin (001) Fe films sandwiched by Au are plotted by closed circles.[25] The x dependence of the higher energy peak is quite similar to that of the ultrathin Fe layer, although the latter appears at slightly lower energies. This deviation may be attributed to the formation of a new band structure in the superlattices for smaller x. The quantum confinement structure has been associated with the transition between $3d$ bands in a Fe layer. On the other hand, as described in Sec. IV, the distinct structure around 4 eV in the $L1_0$ Fe–Au alloy has been assigned to the transition between the Au $5d$ band and the Fe $3d$ band. The change from the quantum confinement scheme to the band scheme seems to be continuous. Further theoretical studies are necessary to explain this continuous turnover between these two cases.

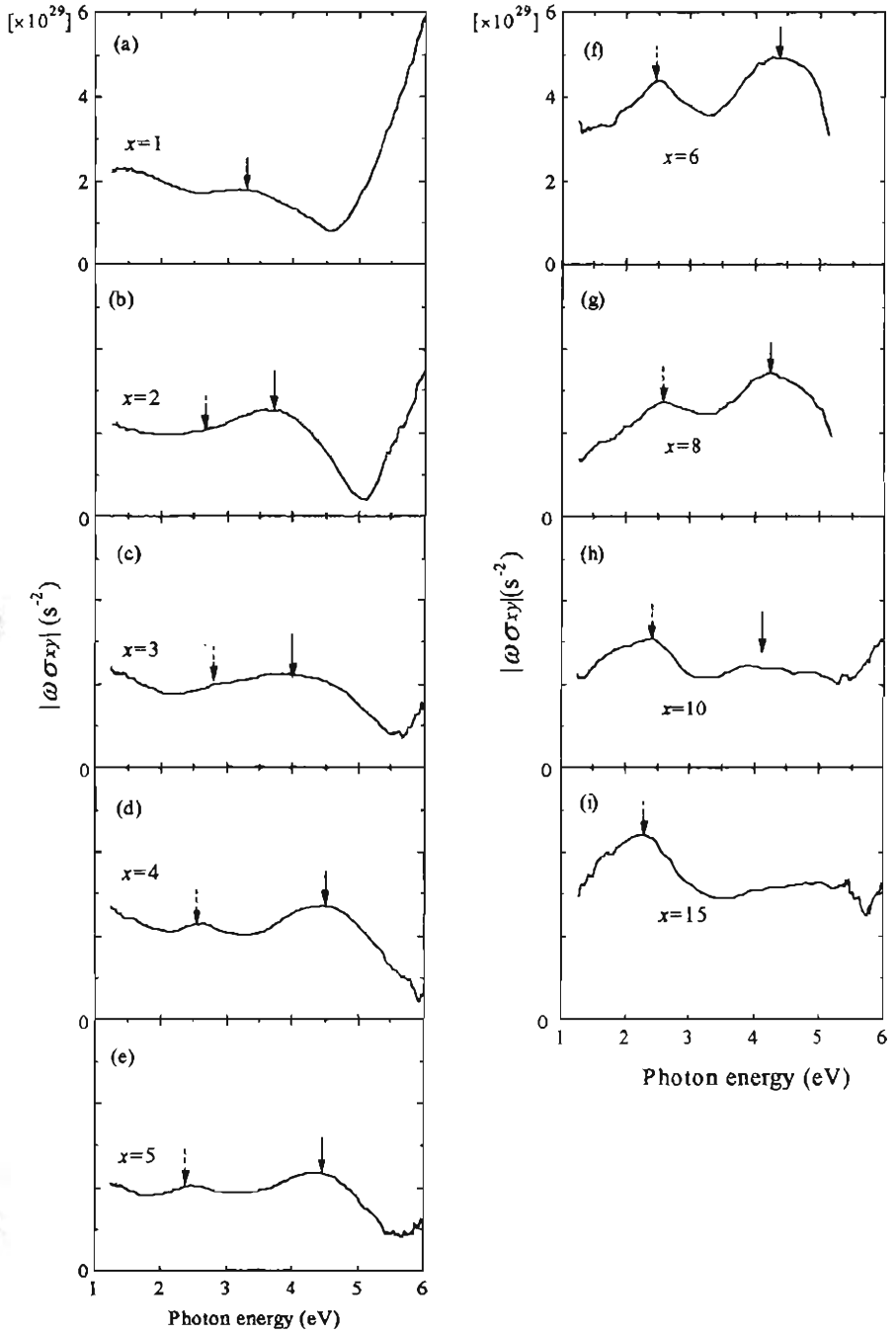

FIG. 14. Spectra of $|\omega\sigma_{xy}|$ in $[\mathrm{Fe}\,(x\mathrm{ML})/\mathrm{Au}\,(x\mathrm{ML})]_N$ $(x=1-15)$ superlattices.

On the contrary, the low-energy peak observed around 2.5 eV may be attributed to the transition specific to Fe. The peak energy shows a systematic shift towards lower energies and is believed to approach the peak position, 1.6 eV, of bulk Fe.

VII. MOKE SPECTRA IN THE FE/AU SUPERLATTICE WITH NONINTEGER MODULATION

For noninteger values of x, the 001 diffraction line of the $L1_0$-type structure in the $[\mathrm{Fe}\,(1\,\mathrm{ML})/\mathrm{Au}\,(1\,\mathrm{ML})]_{100}$ superlattice splits into two separate peaks, the position of which undergoes a systematic change with increasing x. As was discussed in Sec. VI the XRD profiles can successfully be simulated by calculations assuming complete layer-by-layer growth with structural coherence throughout the sample.

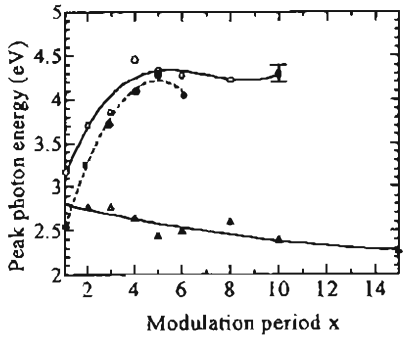

FIG. 15. Plot of peak energies of $|\omega\sigma_{xy}|$ spectra as a function of modulation period x. The open circles denote the high-energy (3–5 eV) structures in the Fe/Au superlattices and the closed circles are Au/Fe/Au sandwiches (Ref. 24). The open triangles show the energy positions of the low-energy (around 2.4 eV) peak in the superlattices.

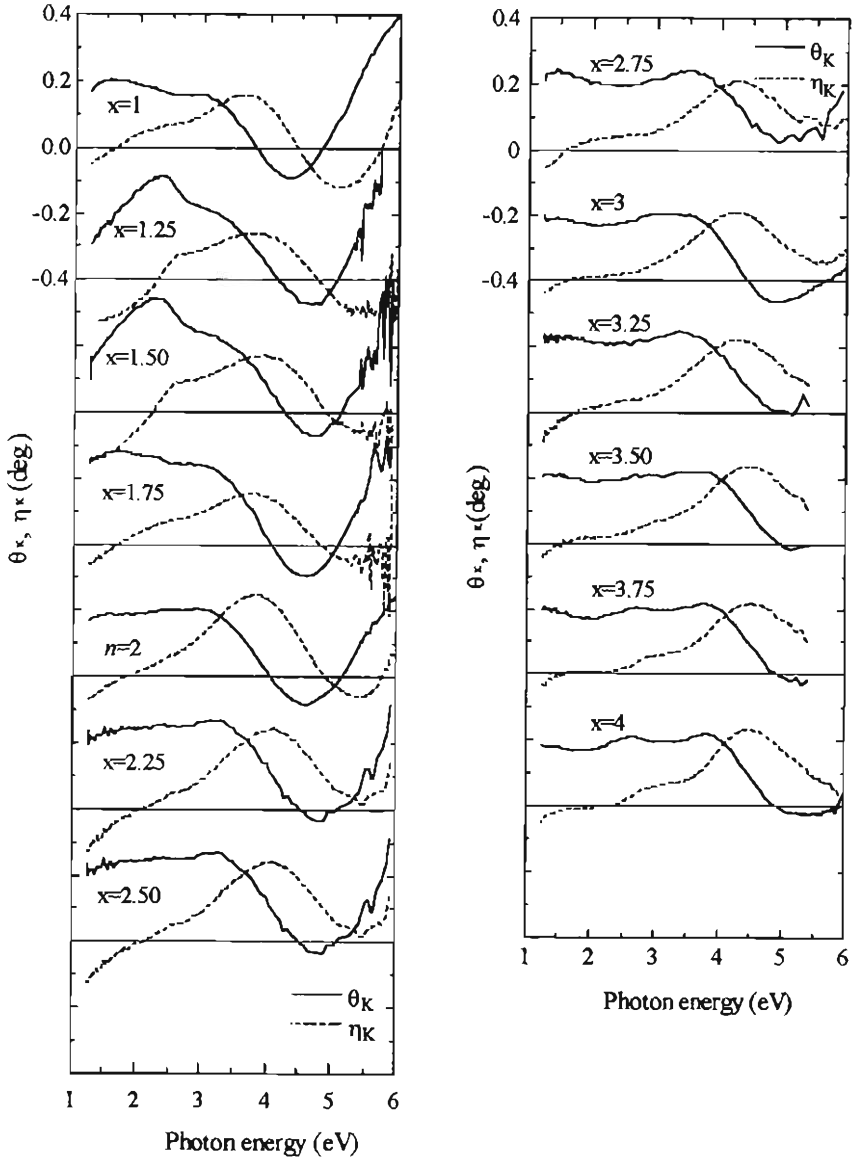

FIG. 16. Spectra of the MOKE in $[\mathrm{Fe}\,(x\mathrm{ML})/\mathrm{Au}\,(x\mathrm{ML})]_N$ for $x=1$, 1.25, 1.5, 1.75, 2, 2.25, 2.5, 2.75, 3, 3.25, 3.5, 3.75 and 4. The Kerr rotation and Kerr ellipticity are plotted by solid and dotted curves, respectively.

Figure 16 shows MOKE spectra of Fe (xML)/Au (xML) for $x=1$, 1.25, 1.5, 1.75, 2, 2.25, 2.5, 2.75, 3, 3.25, 3.5, 3.75 and 4, where Figs. 16(a) and 16(b) corresponds to Kerr rotation and Kerr ellipticity, respectively. Here spectra for $x=1$, 2, 3 and 4 are taken from the magneto-optical spectra described earlier. For two specimens with $x=1.25$ and 1.5 the magneto-optical spectra show a peak around 2.4 eV. It is found that in these samples Kerr rotation and ellipticity spectra are influenced by the diagonal dielectric constants of the Au underlayer since the total thickness of the superlattice was as thin as 13.4 and 15.7 nm, respectively. The samples, except for $x=1.25$ and 1.5, are sufficiently thick so that they are free from the optical effect of the Au underlayer. From the MOKE spectra, $\omega\sigma_{xy}$ was calculated, which is free of the effect of the Au underlayer, using dielectric functions determined by Kramers-Kronig analysis of the reflectivity spectra. For the sake of comparison with Fig. 14, the absolute value $|\omega\sigma_{xy}|$ was calculated and is illustrated in Fig. 17. We find that the structure in the *high-energy* (3.5–5 eV) region shows a monotonic variation for fractional values between the integer modulation. However, the spectra show a strong oscillatory variation with x in the *low-energy* region (less than 3 eV). Figure 18 illustrates the dependence of $|\omega\sigma_{xy}|$ on the modulation period x including noninteger values between $x=1$ and 4 for $\hbar\omega=1.5$, 2.0 and 2.5 eV. An oscillatory variation of $|\omega\sigma_{xy}|$ with the modulation period is observed for all three photon energies. Well-defined peaks are observed at $x=1.75$ and 2.75, and valleys at $x\sim1.5$, 2.5 and 3.5, with the amplitude of oscillation diminishing as x increases. The modulation periods for which the MO effect takes maximum values are slightly different from those in the perpendicular magnetic anisotropy ($t_{\mathrm{Fe}}\times K_{\perp}$).[12] The difference may be explained by the fact that the magnetic anisotropy is related to the ground state of the electronic structure, while the magneto-optical effect is related to both the ground and the excited states.

Here we give a brief discussion of the low-energy spectrum that exhibits an oscillatory behavior with varying layer thickness. The long-range structural coherence shown in Fig. 4 may add a new period of longer sequence to the repetition of layers, which in turn introduces so-called zone folding to the original Brillouin zone. Another possibility is the forma-

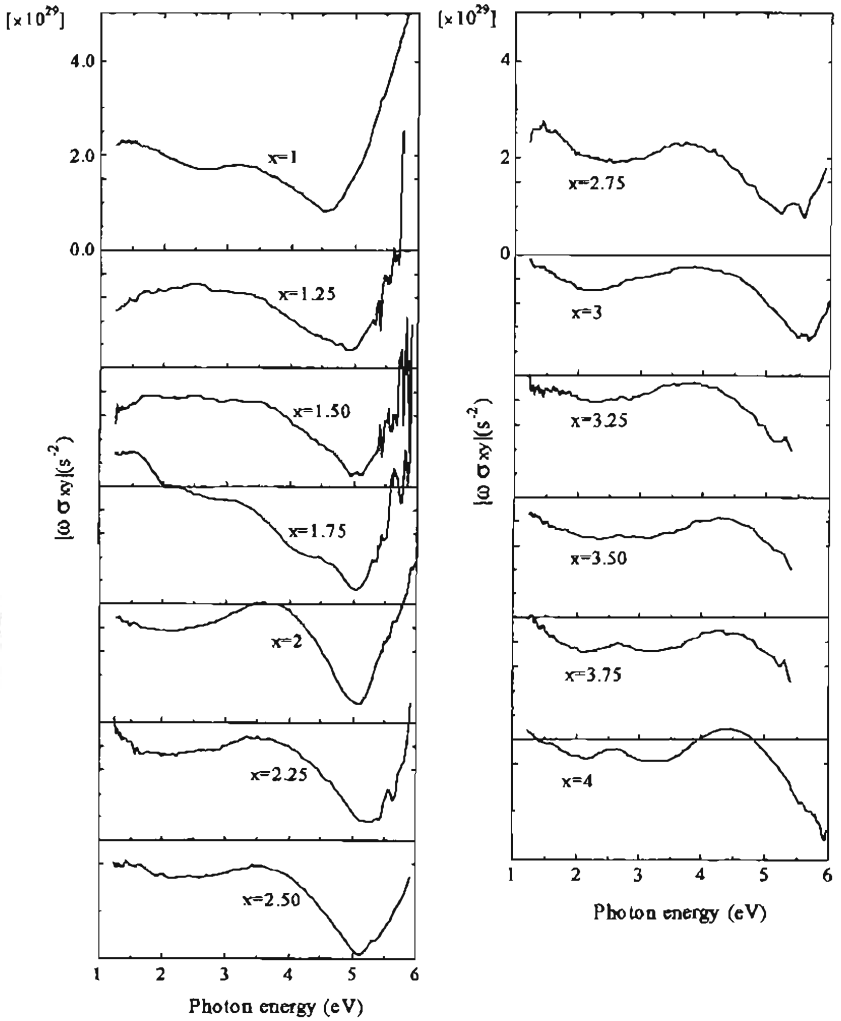

FIG. 17. Spectra of the absolute value $|\omega\sigma_{xy}|$ for $x=1$, 1.25, 1.5, 1.75, 2, 2.25, 2.5, 2.75, 3, 3.25, 3.5, 3.75 and 4.

tion of spontaneous lateral order in the plane perpendicular to the direction of stacking, which may introduce a new electronic structure in the lateral direction. We believe that the new electronic structures produced by the appearance of a lateral structure are responsible for the spectral feature that appears in the fractional superlattices. In semiconductor alloys, the occurrence of either short-range or long-range ordering introduces a considerable change in both the band structure and the crystal symmetry.[26,27] Detailed structural analysis in the lateral direction is necessary to establish a model for the electronic structures of noninteger superlattices. To that end, high resolution transmission electron microscopy (HRTEM), extended x-ray absorption fine structure (EXAFS) analysis and scanning tunneling microscopy (STM) studies are underway.

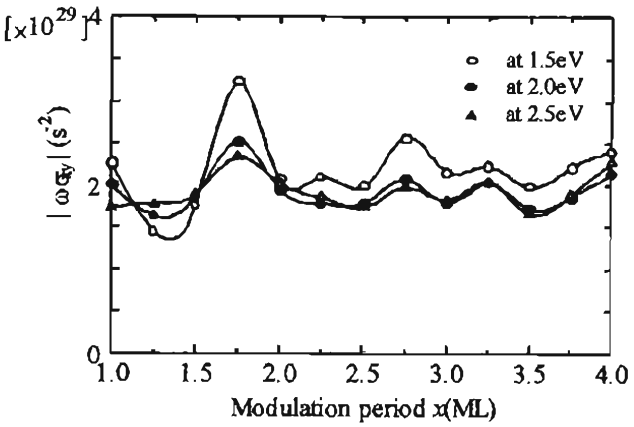

FIG. 18. Dependence of $|\omega\sigma_{xy}|$ on the modulation period x in the fractional superlattices with $1 \leqslant x \leqslant 3$ for photon energies $\hbar\omega = 1.5$, 2.0 and 2.5 eV.

VIII. CONCLUSION

MOKE spectra were measured in $[\mathrm{Fe}(x\mathrm{ML})/\mathrm{Au}(x\mathrm{ML})]_N$ superlattices with integer and noninteger values of x, from which off-diagonal elements of the conductivity tensor were calculated using optical constants from reflectivity spectra determined by the Kramers-Kronig relation. A prominent structure of the spectra of $|\omega\sigma_{xy}|$, which is not present in pure Fe is observed at the photon energy 3.6 eV in the [Fe (1 ML)/Au (1 ML)] superlattice. The energy position of the structure shifts towards higher energies with increasing modulation period x. The structure is associated with a transition from the Au $5d\downarrow$ to the Fe $3d\downarrow$ states according to a band calculation. The MOKE spectra were compared with those in ultrathin Fe layers. It seems there is a continuous turnover between the band states and the quantum confined states. MOKE spectra of $[\mathrm{Fe}(x\mathrm{ML})/\mathrm{Au}(x\mathrm{ML})]_N$ superlattices with noninteger values of x showed the presence of a

low-energy structure, which oscillates with respect to x. This oscillatory behavior was compared with similar oscillatory behavior in the magnetic anisotropy.

ACKNOWLEDGMENTS

This work was supported in part by a Grant-in-Aid for Scientific Research from the Ministry of Education, Science, Sports and Culture. This work was also performed under the interuniversity cooperative research program of the Institute for Materials Research, Tohoku University. The authors are indebted to K. Himi (Tohoku University) for his assistance in sample preparation and to Professor T. Saito (Tokyo University of Agriculture and Technology) for his help in the spectroscopic ellipsometry measurements. They express their gratitude to Dr. D. Book (Tohoku University) for critical reading of the manuscript.

[1] *Ultrathin Magnetic Structures*, edited by J. A. C. Bland and B. Heinrich (Springer, Berlin, 1994), Parts I and III.
[2] Y. Suzuki, T. Katayama, W. Geerts, P. Bruno, and H. Sawada, Mater. Res. Soc. Symp. Proc. **382**, 237 (1995).
[3] K. Takanashi, S. Mitani, M. Sano, H. Fujimori, H. Nakajima, and A. Osawa, Appl. Phys. Lett. **67**, 1016 (1995).
[4] S. Mitani, K. Takanashi, H. Nakajima, K. Sato, R. Schreiber, P. Grünberg, and H. Fujimori, J. Magn. Magn. Mater. **156**, 7 (1996).
[5] K. Sato, T. Kondo, J. Abe, H. Ikekame, M. Sano, K. Takanashi, and H. Fujimori, J. Magn. Soc. Jpn. **20**, 197 (1996).
[6] H. Nakazawa, S. Mitani, K. Takanashi, H. Nakajima, A. Osawa, and H. Fujimori, J. Magn. Soc. Jpn. **20**, 353 (1996) (in Japanese).
[7] K. Takanashi, S. Mitani, H. Nakajima, and H. Fujimori, *Digest of the 15th International Colloq. on Magnetic Films and Surfaces, Sunshine Coast, August 1997*, p. 240.
[8] W. J. M. de Jonge, P. J. H. Bloemen, and F. J. A. den Broeder, in Ref. 1, Part I, Chap. 2.3, p. 650.
[9] K. Sato, J. Abe, H. Ikekame, K. Takanashi, S. Mitani, and H. Fujimori, J. Magn. Soc. Jpn. **20**, 35 (1996).
[10] K. Takanashi, S. Mitani, H. Fujimori, K. Sato, and Y. Suzuki, J. Magn. Magn. Mater. **177–181**, 1199 (1998).
[11] M. Yamaguchi T. Kusakabe, K. Kyuno, and S. Asano, Physica B (submitted).
[12] S. Mitani, K. Takanashi, Y. Shigemoto, and H. Fujimori, Jpn. J. Appl. Phys. Part 2 **36**, L1045 (1997).
[13] K. Takanashi, S. Mitani, Y. Shigemoto, K. Himi and H. Fujimori, in Ref. 7, p. 96.
[14] K. Takanashi, S. Mitani, K. Himi, and H. Fujimori, Appl. Phys. Lett. **72**, 737 (1998).
[15] K. Sato, E. Takeda, M. Akita, S. Mitani, K. Takanashi, and H. Fujimori, J. Magn. Soc. Jpn. **22**, 193 (1998).
[16] K. Sato, H. Hongu, H. Ikekame, Y. Tosaka, M. Watanabe, K. Takanashi, and H. Fujimori, Jpn. J. Appl. Phys., Part 1 **32**, 989 (1993).
[17] P. N. Argyres, Phys. Rev. **97**, 334 (1955).
[18] H. Feil and C. Haas, Phys. Rev. Lett. **58**, 65 (1987).
[19] K. Ohta, A. Takahashi, T. Deguchi, T. Hyuga, S. Kobayashi, and H. Yamaoka, SPIE **382**, 252 (1983).
[20] G. S. Krinchik and V. A. Artemjev, Sov. Phys. JETP **26**, 1080 (1968).
[21] J. L. Erskine and E. A. Stern, Phys. Rev. B **8**, 1239 (1973).
[22] P. Hohenberg and W. Kohn, Phys. Rev. B **136**, 864 (1964); W. Kohn and L. J. Sham, Phys. Rev. A **140**, 1133 (1965).
[23] C. S. Wang and J. Callaway, Phys. Rev. B **9**, 4897 (1974).
[24] Y. Suzuki, T. Katayama, S. Yoshida, K. Tanaka, and K. Sato, Phys. Rev. Lett. **68**, 3355 (1992).
[25] W. Geerts, Y. Suzuki, T. Katayama, K. Tanaka, K. Ando, and S. Yoshida, Phys. Rev. B **50**, 12581 (1994).
[26] J. Mirecki Millunchick, R. D. Twesten, S. R. Lee, D. M. Follstaedt, E. D. Jones, S. P. Ahrenkiel, Y. Zhang, H. M. Cheong, and A. Mascarenhas, MRS Bull. **22**, 38 (1997).
[27] A. Zunger and S. Mahajan, in *Handbook of Semiconductors*, edited by T. S. Moss (Elsevier Science, Amsterdam, 1994,) Vol. 3, p. 1399.